molbank

MDPI

Short Note

trans-Dihydroxo[5,10,15,20-tetrakis(3-pyridinium) porphyrinato]tin(IV) Nitrate

Nirmal Kumar Shee and Hee-Joon Kim *

School of Chemical Materials Engineering, Kumoh National Institute of Technology, Gumi 39177, Republic of Korea; nirmalshee@gmail.com
* Correspondence: hjk@kumoh.ac.kr; Tel.: +82-54-4787822

Abstract: The treatment of *trans*-dihydroxo[5,10,15,20-tetrakis(3-pyridyl)porphyrinato]Sn(IV) or [$Sn(OH)_2$(TPyP)] with 1% nitric acid in a mixture of water and acetone resulted in the formation of an ionic complex **1** [$Sn(OH)_2(TPy^HP)](NO_3)_4$. Complex **1** was fully characterized by ^{1}H NMR spectroscopy, elemental analysis, UV-vis spectroscopy, powder X-ray diffraction, fluorescence spectroscopy, FT-IR spectroscopy, and single-crystal X-ray crystallography. X-ray crystallographic analysis confirmed that each peripheral pyridyl N atom is protonated to form tetra-cationic species $\{Sn(OH)_2(TPy^HP)\}^{4+}$ stabilized by four NO_3^- counter anions. Intermolecular hydrogen bonding interaction between axial hydroxo ligands leads to the formation of a 1D porphyrin array. Nitrate anions also involve hydrogen bonding interactions with axial hydroxo ligands and the peripheral pyridinium groups.

Keywords: Sn(IV) porphyrin; ionic complex; supramolecular assembly; hydrogen bonding

1. Introduction

In recent years, pyridyl-functionalized free-base and metalloporphyrins have been extensively used to fabricate metal–organic frameworks [1], multiporphyrin arrays [2], nanostructures [3], and coordination polymers [4]. Introducing pyridyl-functional groups onto the peripheral positions of porphyrin moieties enables them to react with several transition metal ion connectors and fabricate hybrid organic−inorganic coordination frameworks of varying porosity and topology. Various noncovalent intermolecular interactions such as hydrogen bonding, metal–ligand coordination, and π-π stacking have been primarily responsible for the self-assembly of porphyrins. Researchers have recognized these supramolecular architectures due to their tunable coordination characteristics and attractive optical and electronic properties. Moreover, these compounds have been used in various important applications such as H_2 generation [5], CO_2 reduction [6], solar energy conversion [7], gas separation and storage [8], photodynamic therapy [9], chemical sensor [10], catalysis [11], and water treatments [12]. Among the pyridyl-functionalized metalloporphyrins, Sn(IV)-porphyrin is an important building block for fabricating self-assembled supramolecular architectures [13–17], because its axial positions strongly embrace oxyanion ligands [18–21].

Among the several supramolecular architectures, ionic self-assemblies are achieved through strong electrostatic interactions from the combination of structurally different ionic species with opposite charges [22–25]. Previously, Kim et al. reported several pyridyl-functionalized octahedral Sn(IV)porphyrin-based ionic self-assemblies to fabricate photofunctional nanomaterials [26–28]. Herein, we report an ionic complex derived from the treatment of *trans*-dihydroxo [5,10,15,20-tetrakis(3-pyridyl)porphyrinato]Sn(IV),

check for updates

Academic Editor: R. Alan Aitken

Received: 2 May 2025
Revised: 24 May 2025
Accepted: 26 May 2025
Published: 27 May 2025

Citation: Shee, N.K.; Kim, H.-J. *trans*-Dihydroxo[5,10,15,20-tetrakis(3-pyridinium)porphyrinato]tin(IV) Nitrate. *Molbank* **2025**, *2025*, M2014. https://doi.org/10.3390/M2014

$[Sn(OH)_2(TPyP)]$, with 1% aqueous nitric acid solution. X-ray crystal structure disclosed that intermolecular hydrogen bonding is responsible for the self-assembly of the ionic tin(IV)porphyrin complex. This report could provide new insight for developing porphyrin-based ionic self-assembled supramolecular architectures.

2. Results and Discussion

2.1. Synthesis

An ionic tin(IV) porphyrin complex $[Sn(OH)_2(TPy^HP)](NO_3)_4$ (**1**) was prepared from the treatment of *trans*-dihydroxo[5,10,15,20-tetrakis(3-pyridyl)porphyrinato]Sn(IV) or $[Sn(OH)_2(TPyP)]$ with 1% aqueous solution of nitric acid, followed by crystallization with the addition of acetone [26] (Scheme 1). Complex **1** was fully characterized using elemental analysis, FT-IR spectroscopy, UV-vis spectroscopy, fluorescence spectroscopy, powder X-ray diffraction, ^{1}H NMR spectroscopy, and single-crystal X-ray crystallography.

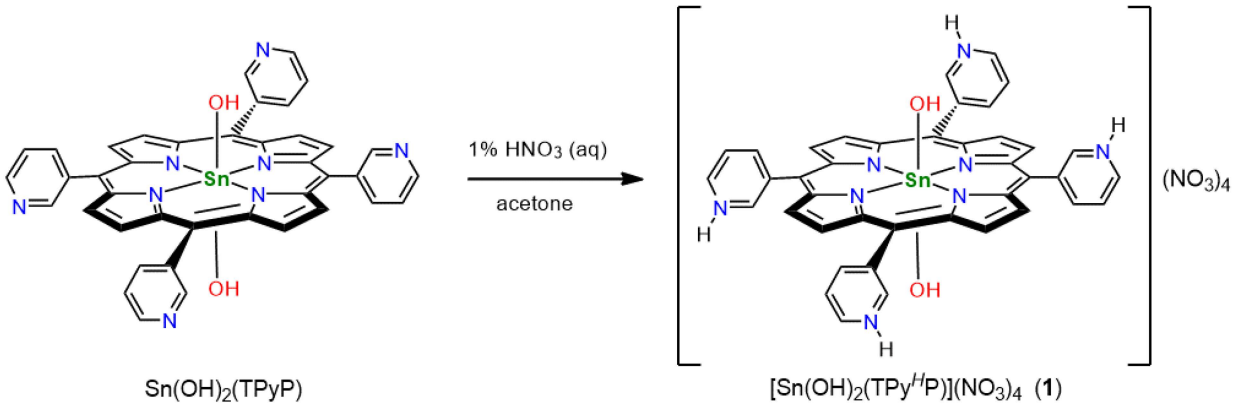

Scheme 1. Synthetic procedure of ionic Sn(IV)porphyrin complex **1**.

2.2. X-Ray Crystal Structure Determination

Plate-shaped wine-colored single crystals of complex **1** were obtained through the slow diffusion of acetone into an aqueous HNO_3 solution (1%) of $[Sn(OH)_2(TPyP)]$ within 7 days. All crystallographic refinement parameters and structural data are summarized in Table S1. Specific bond lengths and bond angles are given in Table S2.

The X-ray crystal structure of **1** revealed that two symmetrically non-equivalent units of caionic Sn(IV)-porphyrin are present per unit cell. The molecular structure of one of them is given in Figure 1. Each Sn(IV) center was octahedrally six-coordinated. The equatorial plane was occupied by four N atoms of the porphyrin ring. On the other hand, the axial positions were connected by the O atoms of the two hydroxo ligands. All the peripheral pyridyl N atoms are protonated to generate tetra-cationic Sn(IV)porphyrin species $[Sn(OH)_2(TPy^HP)]^{4+}$. The overall tetra-cationic charge was balanced by four nitrate (NO_3^-) counter-anions. It is interesting to note that the treatment of *trans*-dihydroxo[5,10,15,20-tetrakis(4-pyridyl)porphyrinato]Sn(IV) with a 1% nitric acid aqueous solution led to the generation of a hexa-cationic $[Sn(OH_2)_2TPy^HP]^{6+}$ species held by six NO_3^- counter-anions [26]. In another comparison, the HSO_4^- and $H_2PO_4^-$ moieties were found to be coordinated to the Sn(IV) center of [5,10,15,20-tetrakis (4-pyridinium)porphyrinato]tin(IV) complex in the H_2SO_4 [28] and H_3PO_4 [12] treatments, respectively. In the case of the first molecule, the axial bond lengths of Sn1-O were found to be 2.091(8) Å. The two equivalent Sn1–N bonds were measured to have lengths of 2.088(9) and 2.105(9) Å. Therefore, the average bond length was calculated to be 2.097 Å and was slightly longer than that found for the $[Sn(OH_2)_2TPy^HP]^{6+}$ species (2.083 Å) [26]. On the other hand, in the case of the second molecule, the axial Sn2-O bonds were found to be

2.095(7) Å. The two equivalent Sn2–N bonds were measured to have lengths of 2.090(9) and 2.081(9) Å. Therefore, the average bond length was found to be 2.085 Å for Sn2–N bonds.

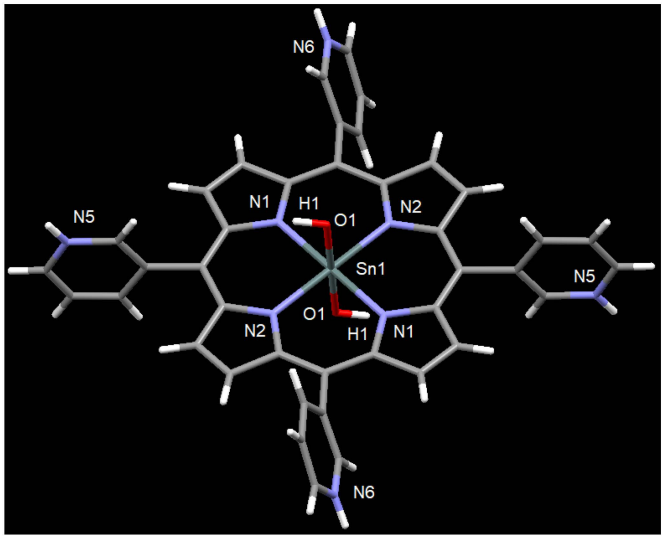

Figure 1. One of the molecular structures of tetra-cationic Sn(IV)porphyrin species $\{Sn(OH)_2(TPy^HP)\}^{4+}$ in **1**. Counter nitrate anions are omitted for clarity.

As depicted in Figure 2, the axial hydroxyl group in one Sn(IV)porphyrin was hydrogen bonded to the oxygen atom of an adjacent Sn(IV)porphyrin framework. The distances from the axial O atom of the hydroxo ligand to the hydrogen-bonded hydroxo ligand in the adjacent Sn(IV)porphyrin moiety were measured to be 1.70 Å (O2···H1) and 2.54 Å (O2···N1), with the O2···H1–O1 angle measured to be 166.9°.

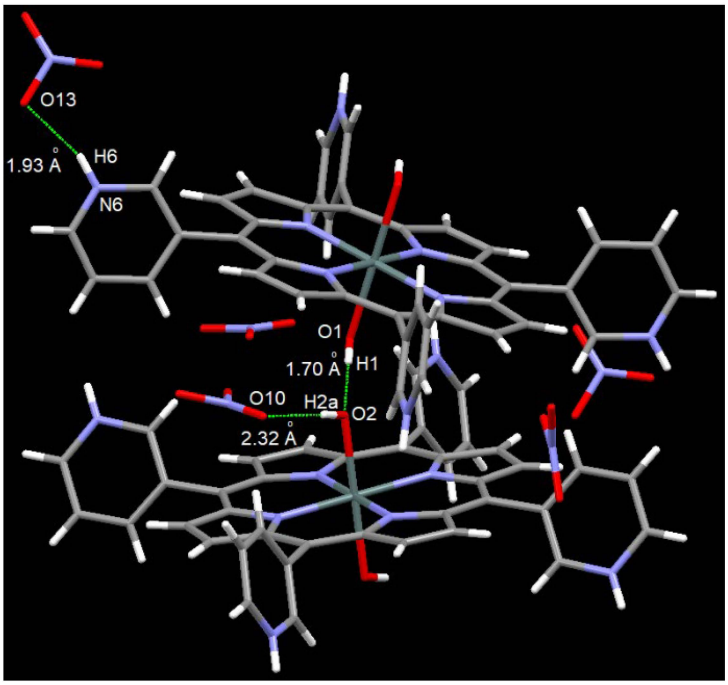

Figure 2. Selected hydrogen bonds in **1** and indicated by dotted green lines along the crystallographic *c*-axis.

Counter nitrate anions were not only electrostatically held by cationic Sn(IV)porphyrin but also by H-bonding. In one case, NO_3^- ions were hydrogen bonded with the axial hydroxo group. The distances were found to be 2.32 Å (O10···H2a) and 3.16 Å (O10···O2),

with the O2···H2a–O10 angle determined to be 175.9°. In another case, NO_3^- ions were hydrogen bonded with the peripheral cationic pyridinium group. The distances were measured to be 1.93 Å (O13···H6) and 2.75 Å (O13···N6), with the N6···H6–O13 angle determined to be 159.5°. Thus, the Sn(IV)porphyrin building blocks were supramolecularly assembled in one-dimensional (1D) frameworks via hydrogen bonding interaction in the crystal structure of **1**. Figures 3 and 4 show a 1D Sn(IV)porphyrin array along the crystallographic *b*- and *c*-axis, respectively.

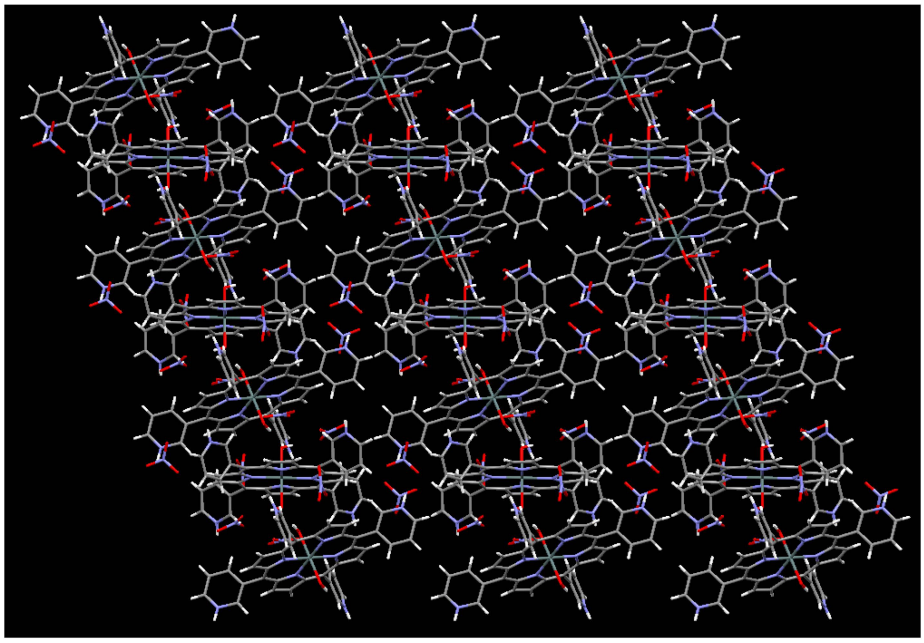

Figure 3. Perspective view of the Sn(IV)porphyrin arrays in **1** along the *b*-axis.

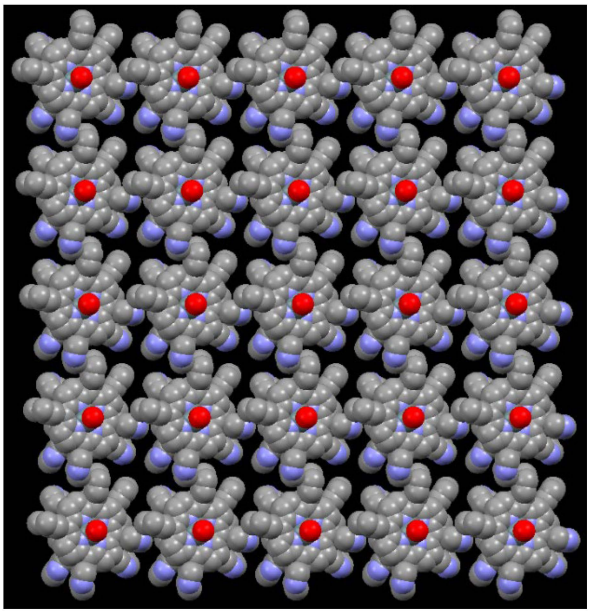

Figure 4. Space-filling representation depicting the regular 1D framework of **1** along the crystallographic *b*-axis. The nitrate anions and hydrogen atoms are excluded for clarity.

2.3. Spectroscopic Characterization

The ^{1}H NMR spectrum of **1** in DMSO-d_6 (Figure S1) reveals that the pyridyl protons (2-position) and *β*-pyrrolic protons resonate as a multiplet at the range from 9.68 ppm to

9.84 ppm. The pyridine protons appear as a singlet at 9.37 ppm (6-position), a singlet at 9.10 ppm (4-position), and another singlet at 8.29 (5-position). In comparison with the ^{1}H NMR spectrum of [Sn(OH)$_2$(TPyP)], pyridyl protons (2-position) appeared as a singlet at 9.43 ppm, a doublet at 9.13 ppm (6-position), a singlet at 8.71 ppm (4-position), and a multiplet at 7.99 ppm (5-position), and β-pyrrolic protons appeared as a singlet at 9.10 ppm [29]. Elemental analysis data (C, H, and N) for **1** also support the molecular derived from the crystal structure analysis.

Solution phase optical characteristics of **1** were observed in water. The UV-visible absorption spectrum shows a sharp Soret absorption band at 416 nm, with Q bands at 512, 551, and 589 nm (Figure S2). Compared with [Sn(OH)$_2$(TPyP)], these peaks appeared at 415, 513, 552, and 590 nm, respectively. The UV-visible absorption spectrum of complex **1** is almost identical to that of [Sn(OH)$_2$(TPyP)]. The fluorescence spectrum of **1** in water are depicted in Figure S3. Complex **1** displays emission bands at 610 and 665 nm. In comparison with the fluorescence spectrum of [Sn(OH)$_2$(TPyP)], these peaks appear at 614 and 664 nm. The fluorescence intensity of **1** is significantly reduced compared to [Sn(OH)$_2$(TPyP)]. We also observe that **1** retains its crystallinity and framework, as evidenced by the powder XRD patterns displayed in Figure S4. The FT-IR spectrum of **1** is shown in Figure S5. The characteristic band for N−O stretching at 1310 cm^{-1} supports the presence of nitrate anions in **1**.

3. Materials and Methods

Trans-dihydroxo[5,10,15,20-tetrakis(3-pyridyl)porphyrinato]tin(IV) or [Sn(OH)$_2$(TPyP)] was synthesized using the previously reported procedure [29]. NMR spectra were recorded on a Bruker BIOSPIN/AVANCE III 400 spectrometer at 293 K (Bruker BioSpin GmbH, Silberstreifen, Rheinstetten, Germany). Elemental analyses were carried out on a ThermoQuest EA 1110 analyzer (Thermo Fisher Scientific, Waltham, MA, USA). UV-Vis absorption spectra were recorded in a Shimadzu UV-3600 spectrophotometer (Shimadzu, Tokyo, Japan). Fluorescence spectra were recorded in a Shimadzu RF-5301PC fluorescence spectrophotometer (Shimadzu, Tokyo, Japan). Powder X-ray diffractometry (XRD) spectra were recorded on a Bruker AXS D8 Advance powder X-ray diffractometer (Bruker, Billerica, MA, USA). FT-IR spectra in KBr pellets (4500 to 500 cm^{-1}) were recorded using a Shimadzu FTIR-8400S spectrophotometer (Shimadzu, Tokyo, Japan).

*3.1. Preparation of trans-Dihydroxo[5,10,15,20-tetrakis(3-pyridinium)porphyrinato]tin(IV) Tetranitrate (**1**)*

[Sn(OH)$_2$(TPyP)] (0.192 g, 0.25 mmol) was added in 3 mL of an aqueous solution of HNO_3 (1%). Acetone (40 mL) was layered over the above aqueous solution for slow diffusion and kept for 7 days in the dark. The plate-shaped wine-colored crystals were filtered and washed with acetone (5 mL), yielding 0.210 g (82%). ^{1}H NMR (400 MHz, DMSO-d$_6$) δ 9.68–9.84 (m, 12H, β-pyrrole + H2-Py), 9.37 (s, 4H, H6-Py), 9.10 (s, 4H, H4-Py), 8.29 (s, 4H, H5-Py). UV–vis (H_2O, nm): λ_{max} (log ε) 416(4.59), 512(2.48), 551(3.26), 589(2.68). Emission (H_2O, λ_{nm}) 610 nm and 665 nm. Anal. Calcd. for $C_{40}H_{30}N_{12}O_{14}Sn$: C, 47.03; H, 2.96; N, 16.46. Found: C, 46.86; H, 3.12; N, 16.34.

3.2. X-Ray Crystal Structure Determination

Crystals from the mother liquor were immersed in Paratone-N hydrocarbon oil on glass fiber, then selected under a microscope, and mounted on the diffractometer at 173 K. The data were collected on a Bruker APEX-II CCD diffractometer (Bruker, Billerica, MA, USA) equipped with a graphite monochromator and Mo-Kα (λ = 0.71073 Å) radiation. The structures were solved by direct methods in SHELXS and refined by full-matrix least-squares on F^2 in the SHELXL program (Version 6.10) [30,31]. Olex2 program

package (version 1.5) [32] has been used for the graphical works. H atoms were affixed in their respective geometric positions. The displacement parameters of the hydrogen atoms were affixed to be 1.2 times higher than the other atoms to which the hydrogen atoms were bonded. All non-hydrogen atoms were refined with independent anisotropic displacement parameters.

4. Conclusions

The treatment of *trans*-dihydroxo[5,10,15,20-tetrakis(3-pyridyl)porphyrinato]Sn(IV) or [$Sn(OH)_2$(TPyP)] with 1% nitric acid in a mixture of H_2O and acetone leads to the formation of an ionic complex **1**. X-ray single crystallographic analysis confirmed that each peripheral pyridyl N atom is protonated to form tetra-cationic species $\{Sn(OH)_2(TPy^HP)\}^{4+}$ stabilized by four NO_3^- counter anions. Intermolecular hydrogen bonding interaction between axial hydroxo groups leads to the formation of a 1D porphyrin array. Nitrate anions also involve hydrogen bonding interactions with axial hydroxo groups as well as the peripheral pyridinium groups. These findings can provide new opportunities to fabricate Sn(IV)porphyrin-containing ionic complexes for enrichment in the field of supramolecular chemistry. They also have the potential to be applied as an optical indicator for monitoring pH changes.

Supplementary Materials: The following are available online: Table S1. Crystallographic data and structure refinements for **1**. Table S2. Selected bond lengths [Å] and angles [°] in **1**. Figure S1. ^{1}H NMR spectrum of **1** in DMSO-d_6. Figure S2. UV-Vis spectra of **1** and [$Sn(OH)_2$(TPyP)] in H_2O. Figure S3. Fluorescence spectra of **1** and [$Sn(OH)_2$(TPyP)] in H_2O (λ_{ext} = 550 nm). Figure S4. Powder XRD pattern of **1**. Figure S5. FT-IR spectrum of **1** in KBr pellet.

Author Contributions: Methodology, formal analysis, investigation, data curation, visualization, writing—original draft preparation, software; N.K.S. Conceptualization, project administration, resources, funding acquisition, validation, and editing; H.-J.K. All authors have read and agreed to the published version of the manuscript.

Funding: This work was supported by Kumoh National Institute of Technology (2024~2026).

Institutional Review Board Statement: Not applicable.

Informed Consent Statement: Not applicable.

Data Availability Statement: CCDC 2445000 contains supplementary crystallographic data for this paper. These data can be obtained free of charge via https://www.ccdc.cam.ac.uk/structures/? (or from the CCDC, 12 Union Road, Cambridge, CB2 1EZ, UK; Fax: +44-1223-336033; E-mail: deposit@ccdc.cam.ac.uk).

Conflicts of Interest: The author declares no conflicts of interest.

References

1. Abrahams, B.F.; Hoskins, B.F.; Robson, R. A new type of infinite 3D polymeric network containing 4-connected, peripherally-linked metalloporphyrin building blocks. *J. Am. Chem. Soc.* **1991**, *113*, 3606–3607. [CrossRef]
2. Khodov, I.; Alper, G.; Mamardashvili, G.; Mamardashvili, N. Hybrid multi-porphyrin supramolecular assemblies: Synthesis and structure elucidation by 2D DOSY NMR studies. *J. Mol. Struct.* **2015**, *1099*, 174–180. [CrossRef]
3. Hu, J.S.; Guo, Y.G.; Liang, H.P.; Wan, L.J.; Jiang, L. Three-dimensional self-organization of supramolecular self-assembled porphyrin hollow hexagonal nanoprisms. *J. Am. Chem. Soc.* **2005**, *127*, 17090–17095. [CrossRef] [PubMed]
4. Ring, D.J.; Aragoni, M.C.; Champness, N.R.; Wilson, C. A coordination polymer supramolecular isomer formed from a single building block: An unexpected porphyrin ribbon constructed from zinc(tetra(4-pyridyl)porphyrin). *CrystEngComm* **2005**, *7*, 621–623. [CrossRef]
5. Kellett, R.M.; Spiro, T.G. Cobalt(I) Porphyrin Catalysis of Hydrogen Production from Water. *Inorg. Chem.* **1985**, *24*, 2373–2377. [CrossRef]

6. Liu, H.; Chen, S.; Zhang, Y.; Li, R.; Zhang, J.; Peng, T. An effective Z-scheme hybrid photocatalyst based on zinc porphyrin derivative and anatase titanium dioxide microsphere for carbon dioxide reduction. *Mater. Today Sustain.* **2022**, *19*, 100164. [CrossRef]
7. Daphnomili, D.; Landrou, G.; Prakash Singh, S.; Thomas, A.; Yesudas, K.; Bhanuprakash, K.; Sharma, G.D.; Coutsolelos, A.G. Photophysical, electrochemical and photovoltaic properties of dye sensitized solar cells using a series of pyridyl functionalized porphyrin dyes. *RSC Adv.* **2012**, *2*, 12899–12908. [CrossRef]
8. Ohmura, T.; Setoyama, N.; Mukae, Y.; Usuki, A.; Senda, S.; Matsumoto, T.; Tatsumi, K. Supramolecular porphyrin-based metal–organic frameworks: Cu(II) naphthoate–Cu(II) tetrapyridyl porphine structures exhibiting selective CO_2/N_2 separation. *CrystEngComm* **2017**, *19*, 5173–5177. [CrossRef]
9. Amos-Tautua, B.M.; Songca, S.P.; Oluwafemi, O.S. Application of Porphyrins in Antibacterial Photodynamic Therapy. *Molecules* **2019**, *24*, 2456. [CrossRef]
10. Peng, R.; Offenhäusser, A.; Ermolenko, Y.; Mourzina, Y. Biomimetic sensor based on Mn(III) meso-tetra(N-methyl-4-pyridyl) porphyrin for non-enzymatic electrocatalytic determination of hydrogen peroxide and as an electrochemical transducer in oxidase biosensor for analysis of biological media. *Sens. Actuators B Chem.* **2020**, *321*, 128437. [CrossRef]
11. Xie, M.-H.; Yang, X.-L.; Zou, C.; Wu, C.-D. A Sn^{IV}–Porphyrin-Based Metal-Organic Framework for the Selective Photo-Oxygenation of Phenol and Sulfides. *Inorg. Chem.* **2011**, *50*, 5318–5320. [CrossRef] [PubMed]
12. Shee, N.K.; Kim, H.-J. Self-Assembled Nanostructure of Ionic Sn(IV)porphyrin Complex Based on Multivalent Interactions for Photocatalytic Degradation of Water Contaminants. *Molecules* **2024**, *29*, 4200. [CrossRef] [PubMed]
13. Langford, S.J.; Woodward, C.P. Supramolecular self-assembly of dihydroxy tin(IV) porphyrin stabilized helical water chains. *CrystEngComm* **2007**, *9*, 218–221. [CrossRef]
14. Babu, B.; Soy, R.C.; Mack, J.; Nyokong, T. Non-aggregated lipophilic water-soluble tin porphyrins as photosensitizers for photodynamic therapy and photodynamic antimicrobial chemotherapy. *New J. Chem.* **2020**, *44*, 11006–11012. [CrossRef]
15. Nikoloudakis, E.; Pigiaki, M.; Polychronaki, M.N.; Margaritopoulou, A.; Charalambidis, G.; Serpetzoglou, E.; Mitraki, A.; Loukakos, P.A.; Coutsolelos, A.G. Self-Assembly of Porphyrin Dipeptide Conjugates toward Hydrogen Production. *ACS Sustain. Chem. Eng.* **2021**, *9*, 7781–7791. [CrossRef]
16. Likhonina, A.E.; Mamardashvili, G.M.; Khodov, I.A.; Mamardashvili, N.Z. Synthesis and Design of Hybrid Metalloporphyrin Polymers Based on Palladium (II) and Copper (II) Cations and Axial Complexes of Pyridyl-Substituted Sn(IV)Porphyrins with Octopamine. *Polymers* **2023**, *15*, 1055. [CrossRef]
17. Shee, N.K.; Kim, H.-J. (*trans*-Dihydroxo)Sn(IV)-[5,10,15,20-tetrakis(2-pyridyl)porphyrin]. *Molbank* **2023**, *2023*, M1669. [CrossRef]
18. Kumar, A.A.; Giribabu, L.; Reddy, D.R.; Maiya, B.G. New molecular arrays based on a Tin(IV) porphyrin scaffold. *Inorg. Chem.* **2001**, *40*, 6757–6766. [CrossRef]
19. Shetti, V.S.; Ravikanth, M. Sn(IV) Porphyrin based axial-bonding type porphyrin triads containing heteroporphyrins as axial ligands. *Inorg. Chem.* **2010**, *49*, 2692–2700. [CrossRef]
20. Amati, A.; Cavigli, P.; Demitri, N.; Natali, M.; Indelli, M.T.; Iengo, E. Sn(IV) multiporphyrin arrays as tunable photoactive systems. *Inorg. Chem.* **2019**, *58*, 4399–4411. [CrossRef]
21. Thomas, A.; Ohsaki, Y.; Nakazato, R.; Kuttassery, F.; Mathew, S.; Remello, S.N.; Tachibana, H.; Inoue, H. Molecular Characteristics of Water-Insoluble Tin-Porphyrins for Designing the One-Photon-Induced Two-Electron Oxidation of Water in Artificial Photosynthesis. *Molecules* **2023**, *28*, 1882. [CrossRef] [PubMed]
22. Wang, Z.; Medforth, C.J.; Shelnutt, J.A. Porphyrin nanotubes by ionic self-assembly. *J. Am. Chem. Soc.* **2004**, *126*, 15954–15955. [CrossRef] [PubMed]
23. Martin, K.E.; Wang, Z.; Busani, T.; Garcia, R.M.; Chen, Z.; Jiang, Y.; Song, Y.; Jacobsen, J.L.; Vu, T.T.; Schore, N.E.; et al. Donor-Acceptor Biomorphs from the Ionic Self-Assembly of Porphyrins. *J. Am. Chem. Soc.* **2010**, *132*, 8194–8201. [CrossRef]
24. Martin, K.E.; Tian, Y.; Busani, T.; Medforth, C.J.; Franco, R.; van Swol, F.; Shelnutt, J.A. Charge Effects on the Structure and Composition of Porphyrin Binary Ionic Solids: ZnTPPS/SnTMePyP Nanomaterials. *Chem. Mater.* **2013**, *25*, 441–447. [CrossRef]
25. Koposova, E.A.; Offenhäusser, A.; Ermolenko, Y.E.; Mourzina, Y.G. Photoresponsive Porphyrin Nanotubes of *Meso*-tetra(4-Sulfonatophenyl)Porphyrin and Sn(IV) *meso*-tetra(4-pyridyl)porphyrin. *Front. Chem.* **2019**, *7*, 351. [CrossRef]
26. Jo, H.J.; Kim, S.H.; Kim, H.-J. Supramolecular Assembly of Tin(IV) Porphyrin Cations Stabilized by Ionic Hydrogen-Bonding Interactions. *Bull. Korean Chem. Soc.* **2015**, *36*, 2348–2351. [CrossRef]
27. Kim, H.-J. Assembly of Sn(IV)-Porphyrin Cation Exhibiting Supramolecular Interactions of Anion·Anion and Anion·π Systems. *Molbank* **2022**, *2022*, M1454. [CrossRef]
28. Shee, N.K.; Kim, H.-J. Supramolecular Self-Assembly of the Zwitterionic Sn(IV)-Porphyrin Complex. *Molbank* **2023**, *2023*, M1723. [CrossRef]
29. Jo, H.J.; Jung, S.H.; Kim, H.-J. Synthesis and Hydrogen-Bonded Supramolecular Assembly of Trans-Dihydroxotin (IV) Tetrapyridyl-porphyrin Complexes. *Bull. Korean Chem. Soc.* **2004**, *25*, 1869–1873.
30. Sheldrick, G.M. A short history of SHELX. *Acta Crystallogr. Sect. A Found. Crystallogr.* **2008**, *64*, 112–122. [CrossRef]

31. Bruker. *SHELXTL (Ver. 6.10): Program for Solution and Refinement of Crystal Structures*; Bruker AXS Inc.: Madison, WI, USA, 2000.
32. Dolomanov, O.V.; Bourhis, L.J.; Gildea, R.J.; Howard, J.A.K.; Puschmann, H. OLEX2: A Complete Structure Solution, Refinement and Analysis Program. *J. Appl. Crystallogr.* **2009**, *42*, 339–341. [CrossRef]